PACT-VLA: SPECULATIVE ACTION-CHUNK VERIFICATION WITH PRE-COMMIT OBSERVATIONS

Anonymous authors
Paper under double-blind review

ABSTRACT

Vision-language-action (VLA) policies are commonly deployed with asynchronous inference in real-world settings, where the next action chunk is generated while the robot is still executing the previous one. By the time the new chunk is committed, the robot and scene have changed, so the chunk is conditioned on a stale observation and task success drops sharply as this inference delay grows. Generating multiple candidate chunks could let newer observations inform the final choice, but existing multi-candidate methods either rank candidates with the stale inference-start observation or repeatedly switch between candidates during execution, which can make the executed action sequence discontinuous. Our key insight is that inference delay can be used as decision time. While candidate generation is still underway, candidate selection can reuse the VLA itself to choose the complete action chunk that best fits a later observation. We propose PACT-VLA, a training-free framework that generates candidates from the inference-start observation and selects one using this pre-commit observation. Its scoring function, FlowRes, measures the residual between each candidate's implied flow direction and the velocity predicted by the frozen policy under the pre-commit observation, requiring no separate verifier. A pipelined implementation overlaps observation processing with candidate generation and batches scoring, so selection adds no control-step delay on the evaluated hardware. At a four-step delay, PACT-VLA improves average success by 15.0 percentage points over RTC on Kinetix and by 5.2 points over single-candidate asynchronous execution with GR00T N1.7 on LIBERO, and it further improves existing delay-robust methods. On three real-robot tasks, it raises average success from 60% to 82% over naive asynchronous execution with the same frozen $\pi_{0.5}$ checkpoint.

1 INTRODUCTION

Vision-language-action (VLA) policies (Brohan et al., 2023; Kim et al., 2024; Wen et al., 2024) increasingly predict action chunks rather than individual actions (Li et al., 2024; Liu et al., 2025a; Black et al., 2024; Team et al., 2024), allowing several control steps to be executed from a single policy inference and preserving temporal coherence across consecutive actions (Black et al., 2026; Zhao et al., 2023; Kim et al., 2025). However, action-chunk generation is not instantaneous. While inference is running, the robot continues to act and the surrounding scene may change. Consequently, by the time a newly generated chunk is ready for execution, the observation from which it was generated may already be stale, and the chunk may no longer fit the scene (Black et al., 2026; Tang et al., 2025; Agouzoul, 2026). The challenge is that action generation begins before later changes are observed.

Existing approaches address this challenge in different ways. Future-state methods use information available at inference start to anticipate the conditions under which the next action chunk will be executed (Tang et al., 2025). However, these methods determine the next action chunk before changes during the current inference interval are observed, so the conditions at execution may differ from what was anticipated. A natural alternative is to postpone this decision by keeping multiple candidate action chunks available until more information about the upcoming execution conditions becomes available. However, some test-time sampling methods still rank these candidates using the inference-start observation (Kwok et al., 2025; Jang et al., 2026), so the final choice remains fixed before later changes are observed.

Reviewers: please read the Reviewer Guidelines (iclr.cc/Conferences/2027/ReviewerGuidelines) and the AI Policy for Reviewers (iclr.cc/Conferences/2027/AIPolicyForReviewers). If you used AI to expand, edit, or polish your review, please provide the input text to the LLM. Better still, consider skipping the LLM and submitting your original text: we, and the authors, are much more interested in your unedited thoughts than in what an LLM has to say. AI-assisted or not, you are putting your name and reputation behind your review: LLM-generated falsehoods, hallucinations or misrepresentations are subject to disciplinary action, which may include desk-rejecting all papers you have authored.

DreamChunk (Chen et al., 2026) goes further by using a learned world model to predict a trajectory for each candidate. As new observations arrive during execution, it compares them with these predicted trajectories and repeatedly reselects which candidate to follow. This allows the choice to respond to newly observed changes, but keeping the decision open during execution can cause repeated candidate switching, making the executed action sequence discontinuous, which can hurt task performance. However, sensing continues while the next chunk is being generated, so an observation arriving during inference can already be available before commitment. This leaves open whether such an observation can be used to finalize one complete action chunk before commitment, without switching between candidates during execution.

Our key insight is that inference delay can be used as decision time. While candidate generation is still underway, candidate selection can reuse the VLA itself to choose the complete action chunk that best fits a later observation. We propose PACT-VLA, which realizes this principle by generating a fixed candidate pool from the inference-start observation and selecting one candidate using a pre-commit observation received shortly before execution. To choose among the candidates, PACT-VLA uses the original flow-based VLA policy (Lipman et al., 2022; Black et al., 2024) to evaluate each candidate under the pre-commit observation. We introduce FlowRes, which measures the mismatch between the flow direction implied by each candidate and the direction predicted by the frozen policy under this observation. The candidate with the lowest FlowRes score is selected, and the controller executes actions from the selected chunk until the next planned chunk switch.

Using a pre-commit observation leaves only a short interval for candidate selection before the planned chunk switch. PACT-VLA therefore processes the pre-commit observation while candidate generation is still running and scores all candidates in a single batch. On the evaluated hardware, the full generation-and-selection cycle remains in the same control-step delay bucket as single-candidate generation. Experiments on Kinetix, LIBERO, and three real-robot tasks demonstrate the benefit of this design. At a four-step delay, PACT-VLA improves average success by 15.0 percentage points over RTC on Kinetix and by 5.2 points over single-candidate asynchronous execution with GR00T N1.7 on LIBERO. Across the three real-robot tasks, average success increases from 60% to 82% using the same frozen $\pi_{0.5}$ checkpoint.

Contributions. Our contributions are as follows.

- We propose PACT-VLA, a training-free framework for action selection under inference delay. PACT-VLA uses observations arriving during inference to select one complete action chunk before commitment, reducing the prediction–execution mismatch.
- We introduce FlowRes, a candidate-verification method that reuses the frozen VLA to rank candidates under the pre-commit observation, without additional training or a separate verifier.
- We design a pipelined implementation that overlaps pre-commit observation processing with candidate generation and batches candidate verification.
- Experiments on Kinetix, LIBERO, and real robots show gains across multiple flow-based VLA policies and further improvements when combined with existing delay-robust methods.

2 Background and Motivation

2.1 Flow-Based Action-Chunk Generation under Inference Delay

Action-chunk policies. We consider a Vision-Language-Action (VLA) policy π_θ. At control step t, the policy receives an observation o_t, containing the visual and robot-state information available at that step, together with a language instruction l_t. The policy predicts an action chunk

$$A = [a_0, \ldots, a_{H-1}] \in \mathbb{R}^{H \times d_a}, \tag{1}$$

where H is the action-chunk length and d_a is the action dimension. The actions in A are executed sequentially over multiple control steps (Chi et al., 2025).

We index time by control steps. With an inference delay of d steps, a prediction started at step t becomes available at step $t + d$. During this interval, an asynchronous controller continues executing actions that were committed earlier (Shukor et al., 2025). The new action chunk is therefore

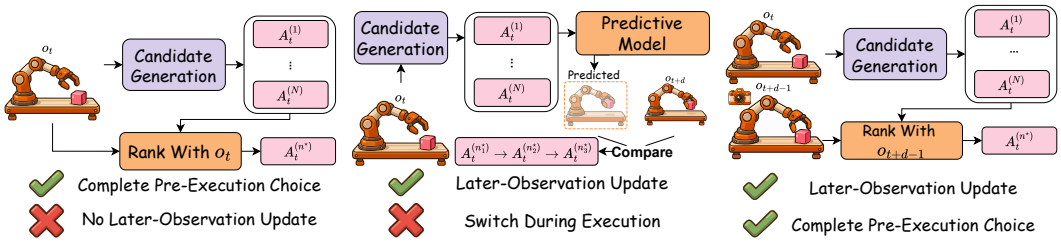

(a) Same-observation ranking (b) World-model-guided reselection (c) Pre-commit ranking (ours)

Figure 1: **Candidate-selection paradigms under delayed execution.** (a) Candidates are generated and ranked using the same observation o_t. (b) A learned predictive model predicts a trajectory for each candidate and repeatedly compares these trajectories with later observations during execution. $n_1^\star$, $n_2^\star$, and $n_3^\star$ denote the candidate indices selected at successive reselection points and may differ as new observations arrive. (c) PACT-VLA uses the original flow policy to rank the fixed candidate pool under the pre-commit observation o_{t+d-1} before the planned chunk switch.

generated from information available at step t but becomes available only at step $t + d$, by which time the robot or scene may have changed. Sensing continues during the same interval.

Flow-based action generation. Flow-based VLA policies generate action chunks by learning a conditional velocity field. Given an action chunk A, Gaussian noise $\epsilon \sim \mathcal{N}(0, I)$, and flow time $\tau \in [0, 1]$, consider the linear interpolation (Liu et al., 2022)

$$x_\tau = (1 - \tau)A + \tau\epsilon, \qquad u_\tau = \frac{\partial x_\tau}{\partial \tau} = \epsilon - A. \tag{2}$$

Here, $x_0 = A$ and $x_1 = \epsilon$. The policy learns an observation- and language-conditioned velocity field (Lipman et al., 2022; 2024) by minimizing

$$\mathcal{L}_{\mathrm{FM}}(\theta) = \mathbb{E}_{(o,l,A)\sim\mathcal{D},\, \tau\sim p_\tau,\, \epsilon\sim\mathcal{N}(0,I)} \left[\left\| v_\theta(x_\tau, \tau \mid o, l) - u_\tau \right\|_2^2 \right], \tag{3}$$

where $\mathcal{D}$ is the training distribution and p_τ is the flow-time sampling distribution.

At inference time, the policy starts from Gaussian noise at $\tau = 1$ and integrates the learned velocity field toward an action chunk as τ decreases to 0. Different noise samples under the same conditioning can produce multiple plausible action chunks, providing a natural source of candidate diversity at test time. In particular, sampling from the inference-start information yields a candidate pool

$$\mathcal{A}_t = \left\{ A_t^{(1)}, \ldots, A_t^{(N)} \right\}, \tag{4}$$

where N is the number of candidate chunks. All candidates are generated from the information available when inference begins. Meanwhile, sensing continues during inference, so later observations may reveal changes in the robot and scene after candidate generation has begun. These changes are not yet observable when generation begins.

2.2 Action Generation and Selection under Inference Delay

Existing methods address the prediction–execution mismatch in different ways. One approach is to predict what the robot will be like when the next chunk is executed. VLASH (Tang et al., 2025) predicts the robot state at the expected execution time and generates the next action chunk based on that prediction. However, the robot may continue to change during inference, so its state at execution may differ from the prediction.

A different approach is to keep multiple candidate action chunks available instead of fixing one chunk immediately. Some test-time sampling methods generate multiple candidates but rank them using the inference-start observation o_t, as shown in Figure 1(a) (Kwok et al., 2025; Jang et al., 2026). Later observations therefore cannot change which candidate is selected. DreamChunk (Chen et al., 2026) goes further by using a learned world model to predict a trajectory for each candidate. As new observations arrive during execution, it compares them with the predicted trajectories and

repeatedly reselects which candidate to follow, as shown in Figure 1(b). This allows the choice to respond to newly observed changes, but keeping the decision open during execution can cause repeated candidate switching, making the executed action sequence discontinuous, which can hurt task performance. Sensing, however, continues while the next chunk is being generated, so a later observation can already be available before commitment. This leaves open whether the inference interval itself can be used to complete the choice of one complete action chunk before commitment.

2.3 Our Insight

Our key insight is that inference delay can be used as a decision-making window. While candidate generation is still ongoing, the selection process can already leverage a later observation, and the VLA itself can determine which complete action chunk best fits that observation before commitment. PACT-VLA builds on this idea by generating a fixed candidate pool from the inference-start observation and completing selection with a pre-commit observation. Section 3 describes how FlowRes reuses the frozen VLA to evaluate the candidates and how pipelined execution completes the selection before the planned chunk switch.

3 Method

3.1 Overview

Figure 2 shows how PACT-VLA realizes the separation between candidate generation and final selection introduced in Section 2.3. At control step t, the VLA begins generating N candidate action chunks $A_t^{(1)}, \ldots, A_t^{(N)}$ using its original candidate-generation procedure and the information available at inference start. These candidates form a fixed pool and are not modified by observations received later.

For delayed execution with $d \geq 1$, the controller is scheduled to switch to the next chunk at step $t + d$. PACT-VLA uses o_{t+d-1}, the observation from one control step before this planned switch, so that one control-step interval remains for observation processing and candidate selection. We call o_{t+d-1} the *pre-commit observation*. The frozen flow policy evaluates the fixed candidates under this observation and assigns FlowRes scores $E_1, \ldots, E_N$. PACT-VLA selects the candidate with

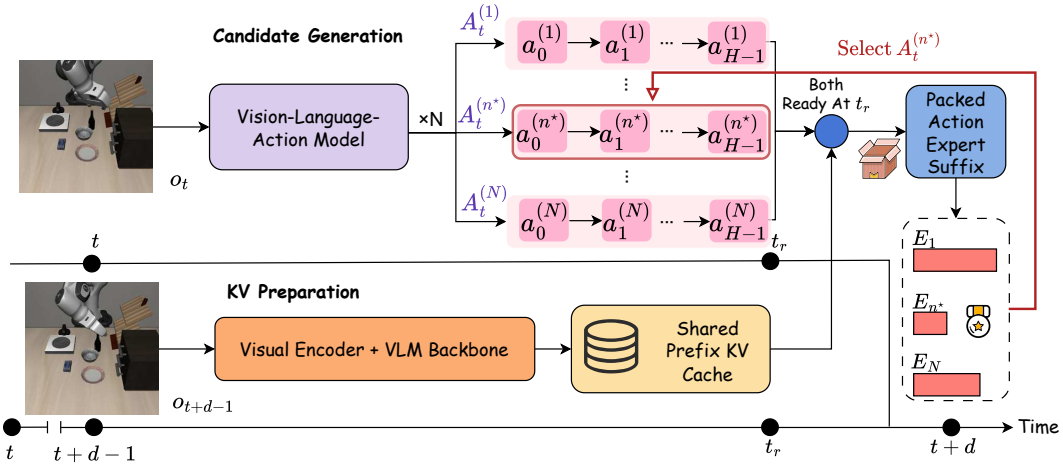

Figure 2: **Overview of PACT-VLA.** At control step t, PACT-VLA uses the policy's original generation procedure to produce a fixed pool of candidate action chunks from the information available at inference start. Before the planned chunk switch at $t + d$, the pre-commit observation o_{t+d-1} is used to evaluate the fixed candidates with FlowRes. The candidate with the lowest score is selected, and the controller switches to this chunk at $t + d$. The lower branch illustrates how pre-commit observation processing can overlap with candidate generation, while the resulting representation is reused for batched candidate scoring.

the lowest FlowRes score. At $t + d$, the controller switches to the selected chunk and executes actions from this chunk until the next planned chunk switch.

Because the pre-commit observation is received close to the planned switch, its processing is pipelined with the remaining candidate-generation computation. For VLA backbones with a reusable visual-language prefix, the visual encoder and VLM backbone process o_{t+d-1} once to prepare a shared prefix KV cache. Once both the candidate pool and the shared cache are ready, all candidates are scored together in a single batched action-expert pass. For flow policies without this module separation, the same verification is implemented as a batched velocity query. The following subsections describe FlowRes verification and pipelined execution in detail.

3.2 FlowRes Candidate Verification

Given the fixed candidate pool $\mathcal{A}_t = \{A_t^{(1)}, \ldots, A_t^{(N)}\}$, PACT-VLA evaluates each candidate under the pre-commit observation. The pointwise velocity residual underlying the flow-matching objective in Section 2.1 compares the flow direction implied by an action chunk with the direction predicted by the policy under a conditioning observation. We use this velocity mismatch as a policy-consistency signal for candidate verification. Figure 3 illustrates the computation for one candidate.

Let $\mathcal{T} = \{\tau_1, \ldots, \tau_M\}$ denote the M verification flow times. For verification, PACT-VLA draws one noise tensor $\epsilon^{\text{ver}} \sim \mathcal{N}(0, I)$ independently of the randomness used to generate the candidates. The same ϵ^{ver} is shared across all candidates and verification flow times (Glasserman & Yao, 1992). Sharing the same verification noise keeps the noise realization fixed across candidate comparisons. Using the same noise across flow times also places the verification points of each candidate on a single interpolation path. For candidate $A_t^{(n)}$ and verification flow time τ_i, we construct

$$
\begin{aligned}
x_{\tau_i}^{(n)} &= (1 - \tau_i) A_t^{(n)} + \tau_i \epsilon^{\text{ver}}, \\
u^{(n)} &= \epsilon^{\text{ver}} - A_t^{(n)}, \\
\hat{v}_{\tau_i}^{(n)} &= v_\theta \left(x_{\tau_i}^{(n)}, \tau_i \mid o_{t+d-1}, l_t \right).
\end{aligned}
\tag{5}
$$

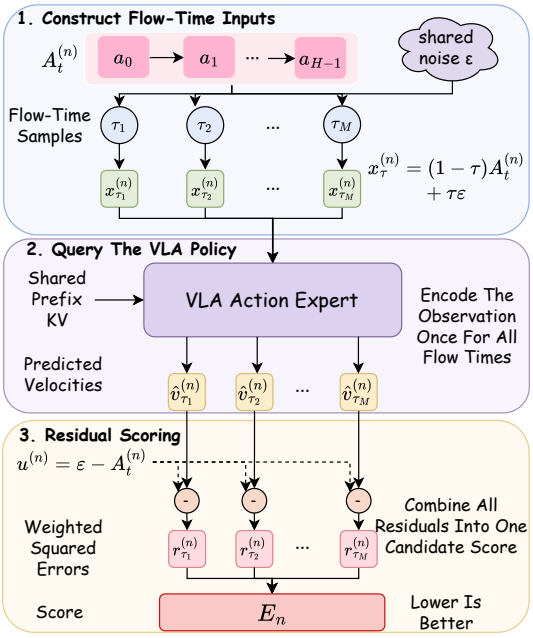

Figure 3: **FlowRes verification of one candidate.** PACT-VLA constructs flow-time inputs from the fixed candidate and shared verification noise, queries the frozen policy under the pre-commit observation, computes the resulting velocity residuals, and aggregates them into candidate score E_n.

Here, $u^{(n)}$ is the flow direction implied by candidate $A_t^{(n)}$, while $\hat{v}_{\tau_i}^{(n)}$ is the direction predicted by the frozen policy for the same flow-time input under the pre-commit observation. Their difference gives the velocity residual for candidate $A_t^{(n)}$ at flow time τ_i under the pre-commit observation.

FlowRes aggregates these residuals over the selected action dimensions, action positions, and verification flow times to obtain one score for each candidate. Let $w_j \geq 0$ denote the weight assigned to action position j, with $w_j = 0$ for positions excluded from verification, and let $\mathbf{m}$ mask the action dimensions included in verification. For each verification flow time τ_i, we compute

$$
\begin{aligned}
r_{\tau_i}^{(n)} &= \sum_{j=0}^{H-1} w_j \left\| \mathbf{m} \odot \left(\hat{v}_{\tau_i, j}^{(n)} - u_j^{(n)} \right) \right\|_2^2, \\
E_n &= \sum_{i=1}^{M} r_{\tau_i}^{(n)}, \\
n^\star &= \arg \min_{1 \leq n \leq N} E_n.
\end{aligned}
\tag{6}
$$

A lower E_n indicates closer agreement between the candidate and the frozen policy under the pre-commit observation. PACT-VLA uses this policy-consistency score to rank the fixed candidate pool and selects the candidate with the lowest E_n for the next planned chunk switch. FlowRes is therefore a policy-consistency score rather than a direct estimate of task success. We evaluate whether this consistency is useful for candidate selection in Section 4.

3.3 Efficient Pipelined Execution

PACT-VLA schedules candidate selection to finish before the planned chunk switch at $t + d$. Since chunk switches occur only at control ticks, meeting this deadline avoids adding another control-step delay.

Candidate generation begins at t and uses shared computation and batching where supported. At $t+d-1$, the controller reads the most recent complete observation packet, which corresponds under our control-step schedule to the pre-commit observation o_{t+d-1}. For backbones with a reusable visual-language prefix, this observation is processed immediately to produce a shared prefix KV cache and can overlap in wall-clock time with the remaining candidate generation. For flow policies without this module separation, the observation is used directly in the later batched velocity query.

Let t_r denote the earliest wall-clock instant at which both the candidate pool and the conditioning required for verification are ready. PACT-VLA then evaluates the $N \times M$ candidate and flow-time inputs from Section 3.2 in one batch and selects $A_t^{(n^\star)}$ according to Eq. 6. Cached backbones use a batched action-expert pass with the shared prefix cache; other flow policies use a batched velocity query.

If selection finishes before $t + d$, the controller switches to $A_t^{(n^\star)}$ at the originally scheduled control tick. Our latency experiments evaluate this timing requirement on the evaluated hardware.

4 Experiments

We design our experiments and analyses to answer the following four questions.

1. Does PACT-VLA improve task success over single-candidate execution and existing delay-robust methods across simulation benchmarks and real-robot tasks?
2. Does FlowRes selection provide gains beyond simply generating more candidates, and how much of the gain comes from the observation used to score them?
3. Does PACT-VLA transfer across inference delays, VLA backbones, benchmarks, and candidate-generation methods?
4. Can PACT-VLA complete candidate selection before the planned chunk switch with practical latency?

4.1 Simulation Evaluation

We evaluate PACT-VLA on Kinetix (Matthews et al., 2025) and LIBERO (Liu et al., 2023). Kinetix tests fast control in dynamic and contact-rich environments, while LIBERO evaluates image-based manipulation with two large flow-based VLA models, $\pi_{0.5}$ (Intelligence et al., 2025) and GR00T N1.7 (Bjorck et al., 2025).

4.1.1 Kinetix

Experimental Setup. Kinetix (Matthews et al., 2025) contains 12 dynamic control tasks involving behaviors such as throwing, catching, and balancing. Following RTC (Black et al., 2026), we use its released behavior-cloning checkpoint with an action-chunk length of $H = 8$. The controller replans every $\max(1, d)$ control steps. All directly evaluated test-time methods use the same checkpoint and execution protocol. PACT-VLA uses $N = 4$ RTC-guided candidates in the main comparison. We evaluate delays $d \in \{0, 1, 2, 3, 4\}$ and report the average success rate across all 12 tasks using 2,048 rollouts for each method and delay.

Compared Methods. We compare PACT-VLA with Naive Async, RTC (Black et al., 2026), BID (Liu et al., 2025b), DreamChunk (Chen et al., 2026), PAINT (Ho et al., 2026), and Training-time RTC (Black et al., 2025). Naive Async performs no delay correction. RTC and PAINT maintain consistency with committed actions, BID selects among sampled chunks using overlap with the previous chunk, DreamChunk uses later observations to match predicted candidate trajectories, and Training-time RTC learns delay handling during training. For RTC, we evaluate the soft-mask variant and also include the reported hard-mask result.

Table 1: **Kinetix success rate (%) across inference delays.** Avg. denotes the mean over $d \in \{1, 2, 3, 4\}$.

Method	d=1	d=2	d=3	d=4	Avg
Naive asynchronous	75.1	71.1	58.7	48.9	63.5
BID (Liu et al., 2025b)	87.9	81.2	68.7	55.8	73.4
RTC (Black et al., 2026)	89.3	84.8	75.0	62.2	77.8
RTC, hard mask (Black et al., 2026)	85.0	81.8	73.2	62.0	75.5
PAINT-Euler (Ho et al., 2026)	85.0	80.4	73.2	63.8	75.6
Training-time RTC (Black et al., 2025)	88.5	86.0	80.0	72.1	81.7
DreamChunk (Chen et al., 2026)	87.0	82.5	70.8	58.5	74.7
PACT-VLA (ours)	**91.1**	**89.4**	**85.6**	**77.2**	**85.8**

Results. As shown in Table 1, PACT-VLA achieves the highest success rate at all four reported delays. Compared with RTC under the same checkpoint and execution protocol, it increases average success from 77.8% to 85.8%. The gain over RTC grows from 1.8 percentage points at $d = 1$ to 15.0 points at $d = 4$. At this longest delay, PACT-VLA reaches 77.2% success, compared with 62.2% for RTC and 48.9% for Naive Async, showing stronger robustness as inference delay increases.

Table 2: **PACT-VLA combined with existing delay-robust methods on Kinetix.** Each pair shows the success rates (%) of a method with and without PACT-VLA.

Proposal / + selection	d=1	d=2	d=3	d=4	Avg
VLASH (Tang et al., 2025)	88.3	86.1	84.0	80.4	84.7
+ **PACT-VLA**	89.4	88.6	87.3	85.0	**87.5** (↑2.8)
DEFLECT (Zhu et al., 2026)	90.8	89.0	88.5	86.1	88.6
+ **PACT-VLA**	91.3	90.3	90.1	88.7	**90.1** (↑1.5)
REMAC (Wang et al., 2026)	88.6	86.0	83.7	76.4	83.7
+ **PACT-VLA**	89.8	87.1	85.3	78.4	**85.2** (↑1.5)

Table 2 further shows that PACT-VLA improves VLASH, DEFLECT, and REMAC at every evaluated delay. Average success increases from 84.7% to 87.5% for VLASH, from 88.6% to 90.1% for DEFLECT, and from 83.7% to 85.2% for REMAC. Each method receives its largest gain at $d = 4$. These results show that PACT-VLA can select from candidate pools produced by different delay-robust proposal methods and further improve their performance.

4.1.2 LIBERO

Experimental Setup. We evaluate PACT-VLA on LIBERO (Liu et al., 2023), which tests image-based manipulation across different spatial arrangements, objects, and task goals. The evaluation covers the Spatial, Object, Goal, and LIBERO-10 suites, with ten tasks in each suite.

We evaluate two independently developed VLAs, $\pi_{0.5}$ (Intelligence et al., 2025) and GR00T N1.7 (Bjorck et al., 2025). For each backbone, the baseline is the corresponding asynchronous policy that generates a single candidate chunk. PACT-VLA uses the same policy, checkpoint, and execution protocol, but generates $N = 8$ candidates and applies FlowRes selection before commitment. We follow the standard evaluation pipeline of each backbone and evaluate delays $d \in \{1, 2, 3, 4\}$. The controller executes the first five actions of each chunk for $\pi_{0.5}$ and the first eight for GR00T

N1.7 before switching to the next chunk. Within each backbone, the baseline and PACT-VLA use the same execution horizon. Each method is evaluated with 500 episodes per suite and delay.

Table 3: **LIBERO success rate (%) for $\pi_{0.5}$ and GR00T N1.7.** Each block compares single-candidate asynchronous execution with PACT-VLA.

	Goal		Spatial		Object		LIBERO-10		Average	
Delay	Single	PACT-VLA	Single	PACT-VLA	Single	PACT-VLA	Single	PACT-VLA	Single	PACT-VLA
					$\pi_{0.5}$					
d=1	92.8	94.6	96.0	94.2	97.0	96.4	91.2	90.4	94.2	93.9 (↓0.3)
d=2	91.4	91.6	85.6	86.4	93.8	95.0	80.2	86.0	87.8	89.8 (↑2.0)
d=3	80.2	85.8	59.0	64.8	89.0	90.0	77.0	78.2	76.3	79.7 (↑3.4)
d=4	68.2	70.0	43.8	47.8	65.0	70.8	62.8	65.2	60.0	63.5 (↑3.5)
					GR00T N1.7					
d=1	93.6	93.2	96.0	96.2	96.4	96.6	87.6	85.2	93.4	92.8 (↓0.6)
d=2	86.2	89.2	88.0	89.6	92.2	93.4	72.6	76.2	84.8	87.1 (↑2.3)
d=3	67.6	73.0	73.0	75.0	82.2	87.0	55.4	62.0	69.6	74.3 (↑4.7)
d=4	52.2	58.2	53.6	56.8	62.6	67.8	36.4	42.6	51.2	56.4 (↑5.2)

Results. Table 3 reveals a clear delay-dependent pattern. At $d = 1$, verification sees the same observation as generation, not an updated view of the scene. PACT-VLA can still select a different chunk, but a lower score under the old observation does not necessarily mean better execution. This selection can help or hurt task success. On LIBERO, average success decreases slightly on both backbones in this setting. At $d = 2, 3, 4$, the pre-commit observation is more recent than the generation observation, and both backbones improve on average. Across the tested delays, the average success-rate gain over single-candidate execution increases with inference delay on both backbones. At $d = 4$, the gain reaches 3.5 percentage points on $\pi_{0.5}$ and 5.2 points on GR00T N1.7.

At $d = 4$, PACT-VLA improves all four LIBERO suites on both backbones. On GR00T N1.7 at this delay, its average success is 4.2 percentage points higher than random selection and 3.8 points higher than FlowRes scoring under the generation observation. All three selectors use $N = 8$ candidates (Appendix D).

4.2 Real-World Evaluation

We deploy an in-house $\pi_{0.5}$ (Intelligence et al., 2025) policy on a bimanual AgileX PiperX platform with two 6-DoF arms. The robot is equipped with three Intel RealSense D435i cameras, including one overhead camera and one wrist camera on each arm. Our system is built on LeRobot (Cadene et al., 2024).

4.2.1 Task Success

Experimental Setup. We use an action-chunk length of $H = 50$ and 10 denoising steps. The robot operates at 30 Hz, and the asynchronous controller requests a new prediction when half of the current action queue remains. Using $\pi_{0.5}$, we compare Naive Async, VLASH, Old-FlowRes, and PACT-VLA. Naive Async, Old-FlowRes, and PACT-VLA use the same frozen task-specific $\pi_{0.5}$ checkpoint obtained by standard SFT. PACT-VLA requires no further training. Naive Async generates a single action chunk, while Old-FlowRes and PACT-VLA each generate $N = 4$ candidates. Old-FlowRes scores them using the observation available at generation start, whereas PACT-VLA uses the pre-commit observation. VLASH is evaluated separately using its own checkpoint.

We evaluate three everyday manipulation tasks. **Toasting Bread** requires placing two slices into a toaster and retrieving them afterward. **Loading Dishwasher** requires loading bowls and a plate into a dishwasher and later returning them to the table. **Pouring Coffee Beans** requires scooping beans onto a plate and pouring them back into the container. For each task, we conduct 50 trials per method and report full-task success, which requires all task sub-goals to be completed.

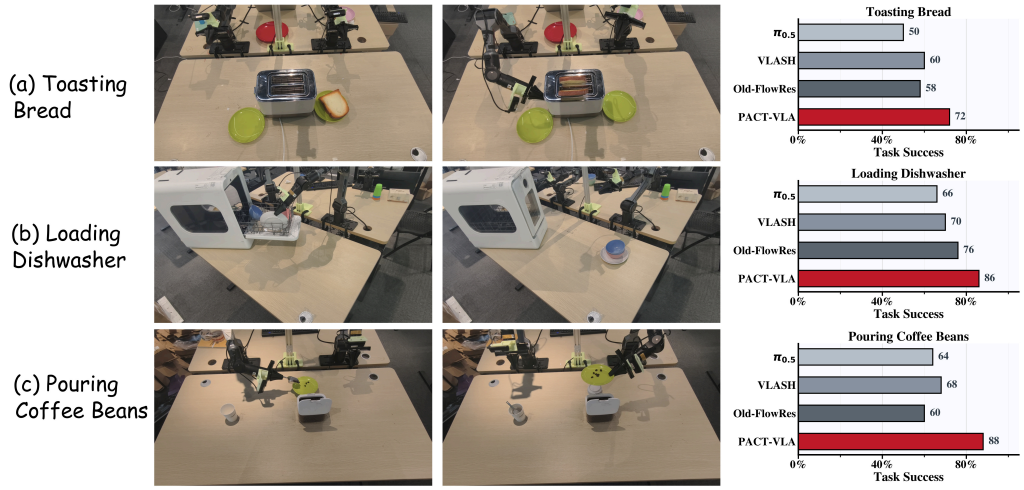

Figure 4: **Real-world evaluation.** Example task stages and full-task success rates (%) for $\pi_{0.5}$ with Naive Async execution, VLASH, Old-FlowRes, and PACT-VLA. Old-FlowRes scores candidates using the generation observation, while PACT-VLA uses the pre-commit observation.

Results. Figure 4 shows that PACT-VLA achieves the highest success rate on all three tasks. Average success is 60.0% for Naive Async, 66.0% for VLASH, 64.7% for Old-FlowRes, and 82.0% for PACT-VLA. Compared with Old-FlowRes, PACT-VLA improves success by 14 percentage points on Toasting Bread, 10 points on Loading Dishwasher, and 28 points on Pouring Coffee Beans, for an average gain of 17.3 points. Since the policy checkpoint, candidate budget, and execution rule are unchanged, this comparison supports using the pre-commit observation for candidate selection. PACT-VLA also achieves 16.0 percentage points higher average success than VLASH in this evaluation.

4.2.2 Deployment Latency

Table 4: **Generation and verification latency across GPUs.** Each entry is the P99 latency measured on that GPU. The control-step delay d is calculated from the listed latency at 30 Hz.

GPU	Generation ($N = 1$)		Generation + Verification ($N = 4$)	
	Latency (ms)	d	Latency (ms)	d
RTX 5090	35.4	2	60.2	2
H100	42.5	2	58.8	2
RTX Pro 6000	48.7	2	64.8	2

Table 4 compares single-candidate generation with four-candidate generation and FlowRes verification across three GPUs. Appendix C resolves the RTX 5090 figure into the stages of one decision cycle.

At 30 Hz, the controller can switch action chunks only every 33.33 ms. On all three GPUs, both configurations take more than one control period but less than two, corresponding to $d = 2$. Thus, although PACT-VLA requires additional computation, the reported runtimes correspond to the same control-step delay as single-candidate generation on each GPU.

5 Conclusion

We presented PACT-VLA, a training-free framework that uses inference delay as decision time for action-chunk selection. While candidate generation is underway, observations arriving during inference can guide the pre-commit choice of one complete action chunk, with FlowRes reusing the frozen flow policy to rank the candidates. Across Kinetix, LIBERO, and three real-robot tasks, PACT-VLA improves delayed execution, complements existing delay-robust methods, and raises real-robot average success from 60% to 82% using the same checkpoint.

AI USE STATEMENT

We used generative AI tools (Claude Code, based on Anthropic's Claude models) throughout this project. In the categories for which ICLR requires disclosure, we used these tools to implement methods, to design and to give feedback on our experimental methodology, to propose and refine hypotheses, to reformat and aggregate evaluation logs, and to interpret results. We did not use generative AI to generate synthetic datasets, to develop theoretical models or conceptual frameworks, or to formulate, support, or write proofs of mathematical claims; these categories are not applicable to this work. In the categories for which disclosure is recommended, we additionally used these tools to write and edit software code, to draft and to edit parts of this paper, to identify and summarise related literature, and to format references.

We have reviewed all AI-assisted work, and we validated the AI-assisted evaluation code against external reference points rather than by inspection alone. Our runs of published baselines are checked against the numbers their authors report, to the precision those numbers can be read off published figures, and an $N{=}1$ control recovers the RTC row through our own execution path (Appendix B); the released $\pi_{0.5}$ LIBERO checkpoint reproduces its published clean success rate on our harness before any of our own machinery is enabled; and where a cell was run under two independent seeds we report their agreement. Implementation errors found this way, including one in an early scoring implementation that silently regressed onto zero-padded action dimensions and one in which replicated candidates aliased a single mutable input, were fixed and every affected result was recomputed.

We take responsibility for the final content of this work, including all text, claims, and artifacts produced with the aid of generative AI.

REFERENCES

Ayoub Agouzoul. Understanding asynchronous inference methods for vision-language-action models. *arXiv preprint arXiv:2605.08168*, 2026.

Johan Bjorck, Fernando Castañeda, Nikita Cherniadev, Xingye Da, Runyu Ding, Linxi Fan, Yu Fang, Dieter Fox, Fengyuan Hu, Spencer Huang, et al. Gr00t n1: An open foundation model for generalist humanoid robots. *arXiv preprint arXiv:2503.14734*, 2025.

Kevin Black, Noah Brown, Danny Driess, Adnan Esmail, Michael Equi, Chelsea Finn, Niccolo Fusai, Lachy Groom, Karol Hausman, Brian Ichter, et al. π_0: A vision-language-action flow model for general robot control. *arXiv preprint arXiv:2410.24164*, 2024.

Kevin Black, Allen Z Ren, Michael Equi, and Sergey Levine. Training-time action conditioning for efficient real-time chunking. *arXiv preprint arXiv:2512.05964*, 2025.

Kevin Black, Manuel Galliker, and Sergey Levine. Real-time execution of action chunking flow policies. *Advances in Neural Information Processing Systems*, 38:33383–33407, 2026.

Anthony Brohan, Noah Brown, Justice Carbajal, Yevgen Chebotar, Xi Chen, Krzysztof Choromanski, Tianli Ding, Danny Driess, Avinava Dubey, Chelsea Finn, et al. Rt-2: Vision-language-action models transfer web knowledge to robotic control. *arXiv preprint arXiv:2307.15818*, 2023.

Remi Cadene, Simon Alibert, Alexander Soare, Quentin Gallouedec, Adil Zouitine, Steven Palma, Pepijn Kooijmans, Michel Aractingi, Mustafa Shukor, Dana Aubakirova, et al. Lerobot: State-of-the-art machine learning for real-world robotics in pytorch. *arXiv preprint*, 2024.

Wenxi Chen, Kaidi Zhang, Chi Lin, Zhiyuan Zhang, Yu She, Yuejiang Liu, Raymond A Yeh, Shaoshuai Mou, and Yan Gu. Dream-chunk: Reactive action chunking with latent world model. *arXiv preprint arXiv:2606.18589*, 2026.

Cheng Chi, Zhenjia Xu, Siyuan Feng, Eric Cousineau, Yilun Du, Benjamin Burchfiel, Russ Tedrake, and Shuran Song. Diffusion policy: Visuomotor policy learning via action diffusion. *The International Journal of Robotics Research*, 44(10-11):1684–1704, 2025.

Paul Glasserman and David D Yao. Some guidelines and guarantees for common random numbers. *Management Science*, 38(6):884–908, 1992.

Trong-Bao Ho, Quang-Tan Nguyen, Thien-Loc Ha, Gia-Binh Nguyen, Viet-Thanh Nguyen, Long Dinh, Minh N Vu, Duy MH Nguyen, An Thai Le, and Ngo Anh Vien. Start right, arrive right: Asynchronous execution via initial noise selection. *arXiv preprint arXiv:2606.19774*, 2026.

Physical Intelligence, Kevin Black, Noah Brown, James Darpinian, Karan Dhabalia, Danny Driess, Adnan Esmail, Michael Equi, Chelsea Finn, Niccolo Fusai, et al. $\pi_{0.5}$: a vision-language-action model with open-world generalization. *arXiv preprint arXiv:2504.16054*, 2025.

Suhyeok Jang, Dongyoung Kim, Changyeon Kim, Youngsuk Kim, and Jinwoo Shin. Verifier-free test-time sampling for vision-language-action models. In *International Conference on Learning Representations*, volume 2026, pp. 139997–140017, 2026.

Moo Jin Kim, Karl Pertsch, Siddharth Karamcheti, Ted Xiao, Ashwin Balakrishna, Suraj Nair, Rafael Rafailov, Ethan Foster, Grace Lam, Pannag Sanketi, et al. Openvla: An open-source vision-language-action model. *arXiv preprint arXiv:2406.09246*, 2024.

Moo Jin Kim, Chelsea Finn, and Percy Liang. Fine-tuning vision-language-action models: Optimizing speed and success. *arXiv preprint arXiv:2502.19645*, 2025.

Jacky Kwok, Christopher Agia, Rohan Sinha, Matt Foutter, Shulu Li, Ion Stoica, Azalia Mirhoseini, and Marco Pavone. Robomonkey: Scaling test-time sampling and verification for vision-language-action models. *arXiv preprint arXiv:2506.17811*, 2025.

Qixiu Li, Yaobo Liang, Zeyu Wang, Lin Luo, Xi Chen, Mozheng Liao, Fangyun Wei, Yu Deng, Sicheng Xu, Yizhong Zhang, et al. Cogact: A foundational vision-language-action model for synergizing cognition and action in robotic manipulation. *arXiv preprint arXiv:2411.19650*, 2024.

Yaron Lipman, Ricky TQ Chen, Heli Ben-Hamu, Maximilian Nickel, and Matt Le. Flow matching for generative modeling. *arXiv preprint arXiv:2210.02747*, 2022.

Yaron Lipman, Marton Havasi, Peter Holderrieth, Neta Shaul, Matt Le, Brian Karrer, Ricky TQ Chen, David Lopez-Paz, Heli Ben-Hamu, and Itai Gat. Flow matching guide and code. *arXiv preprint arXiv:2412.06264*, 2024.

Bo Liu, Yifeng Zhu, Chongkai Gao, Yihao Feng, Qiang Liu, Yuke Zhu, and Peter Stone. Libero: Benchmarking knowledge transfer for lifelong robot learning. *Advances in Neural Information Processing Systems*, 36:44776–44791, 2023.

Songming Liu, Lingxuan Wu, Bangguo Li, Hengkai Tan, Huayu Chen, Zhengyi Wang, Ke Xu, Hang Su, and Jun Zhu. Rdt-1b: a diffusion foundation model for bimanual manipulation. In *International Conference on Learning Representations*, volume 2025, pp. 29982–30009, 2025a.

Xingchao Liu, Chengyue Gong, and Qiang Liu. Flow straight and fast: Learning to generate and transfer data with rectified flow. *arXiv preprint arXiv:2209.03003*, 2022.

Yuejiang Liu, Jubayer Hamid, Annie Xie, Yoonho Lee, Max Du, and Chelsea Finn. Bidirectional decoding: Improving action chunking via guided test-time sampling. In *International Conference on Learning Representations*, volume 2025, pp. 4594–4627, 2025b.

Michael Matthews, Michael Beukman, Chris Lu, and Jakob Foerster. Kinetix: Investigating the training of general agents through open-ended physics-based control tasks. In *International Conference on Learning Representations*, volume 2025, pp. 58515–58564, 2025.

Mustafa Shukor, Dana Aubakirova, Francesco Capuano, Pepijn Kooijmans, Steven Palma, Adil Zouitine, Michel Aractingi, Caroline Pascal, Martino Russi, Andres Marafioti, et al. Smolvla: A vision-language-action model for affordable and efficient robotics. *arXiv preprint arXiv:2506.01844*, 2025.

Jiaming Tang, Yufei Sun, Yilong Zhao, Shang Yang, Yujun Lin, Zhuoyang Zhang, James Hou, Yao Lu, Zhijian Liu, and Song Han. Vlash: Real-time vlas via future-state-aware asynchronous inference. *arXiv preprint arXiv:2512.01031*, 2025.

Octo Model Team, Dibya Ghosh, Homer Walke, Karl Pertsch, Kevin Black, Oier Mees, Sudeep Dasari, Joey Hejna, Tobias Kreiman, Charles Xu, et al. Octo: An open-source generalist robot policy. *arXiv preprint arXiv:2405.12213*, 2024.

Haoxuan Wang, Gengyu Zhang, Yan Yan, Yuzhang Shang, Ramana Kompella, and Gaowen Liu. Real-time robot execution with masked action chunking. In *International Conference on Learning Representations*, volume 2026, pp. 120161–120179, 2026.

Junjie Wen, Minjie Zhu, Yichen Zhu, Zhibin Tang, Jinming Li, Zhongyi Zhou, Chengmeng Li, Xiaoyu Liu, Yaxin Peng, Chaomin Shen, et al. Diffusion-vla: Generalizable and interpretable robot foundation model via self-generated reasoning. *arXiv preprint arXiv:2412.03293*, 2024.

Tony Z Zhao, Vikash Kumar, Sergey Levine, and Chelsea Finn. Learning fine-grained bimanual manipulation with low-cost hardware. *arXiv preprint arXiv:2304.13705*, 2023.

Pengfei Zhou, Shengcong Chen, Di Chen, Jiaxu Wang, Rongjun Jin, Bingwen Zhu, Yike Pan, Songen Gu, Kuanning Wang, Shufeng Nan, et al. τ_0-wm: A unified video-action world model for robotic manipulation. *arXiv preprint arXiv:2606.01027*, 2026.

Yixiang Zhu, Yonghao Chen, Zijie Yang, Yusong Hu, and Xinyu Chen. Deflect: Temporal counterfactual preference learning for delay-robust asynchronous vlas. *arXiv preprint arXiv:2605.19294*, 2026.

A Related Work

Action-Chunk Execution under Inference Delay. Existing methods address delayed execution by improving chunk continuity or adapting the policy to the expected execution state. RTC (Black et al., 2026) uses inpainting guidance to align new predictions with committed actions, while PAINT (Ho et al., 2026) achieves prefix consistency through initial noise selection. VLASH (Tang et al., 2025) uses future-state conditioning, and Training-time RTC (Black et al., 2025) learns to generate chunks from committed action prefixes. REMAC (Wang et al., 2026) learns corrective adjustments through masked action chunking. DEFLECT (Zhu et al., 2026) instead constructs offline preferences from future and stale observations to improve the policy under its deployment input. These approaches primarily change how action chunks are generated. PACT-VLA complements them by keeping their generation procedure and using the pre-commit observation to select among the resulting candidates.

Test-Time Action Selection and Verification. Generating multiple candidates allows a policy to compare alternatives rather than execute its first prediction. Existing approaches differ in the information used for this comparison. BID (Liu et al., 2025b) uses backward coherence and forward contrast to guide candidate selection. RoboMonkey (Kwok et al., 2025) employs a learned VLM verifier, whereas MG-Select (Jang et al., 2026) derives confidence from the policy's action-token distributions. τ_0-WM (Zhou et al., 2026) uses re-denoising consistency to rank candidates under the generation observation. PACT-VLA uses a newer pre-commit observation to verify previously generated candidates, with selection completed before the planned chunk switch. DreamChunk (Chen et al., 2026) also incorporates observations collected after generation. It predicts candidate latent trajectories with a learned world model and matches them against the observed rollout. PACT-VLA instead scores the existing chunks directly with the frozen flow policy under the pre-commit observation. Its distinction is therefore the combination of updated observations and policy-based candidate verification, without requiring a separate learned verifier or predictive model.

B Experimental Settings and Statistical Reporting

Evaluation settings. Table 5 summarizes the main simulation configurations, including the execution protocol, checkpoint, candidate-generation method, candidate count, evaluation count, and execution-noise level. The LIBERO selector comparisons in Appendix D use the GR00T configuration in the last row, with $N{=}1$ for the single-candidate baseline and $N{=}8$ for the three multi-candidate methods.

Table 5: What differs between experiments. "Proposal" is where the N candidates come from. The main PACT-VLA configuration verifies candidates under the pre-commit observation o_{t+d-1}; alternative selectors and verification observations are specified in Appendix D. Evaluation counts are per Kinetix level or LIBERO suite for each method and delay.

Result	Protocol	Ckpt	Proposal	N	Evaluation count	σ
Table 1	continuous, H=8, $d\leq$4	`bc/31`	RTC-guided	4	2048	0.1
Table 2, VLASH	continuous, H=8, $d\leq$4	async5	speculative	1 / 4	2048	0.1
Table 2, DEFLECT	continuous, H=8, $d\leq$4	DEFLECT	speculative	1 / 4	2048	0.1
Table 2, REMAC	continuous, H=8, $d\leq$4	REMAC LoRA	warm-start refine	1 / 4	2048	0.1
Table 3, $\pi_{0.5}$	predict 50, execute 5, $d\leq$4	$\pi_{0.5}$ LIBERO	policy sampling	1 / 8	500	0
Table 3, GR00T	predict 16, execute 8, $d\leq$4	GR00T N1.7 per suite	policy sampling	1 / 8	500	0

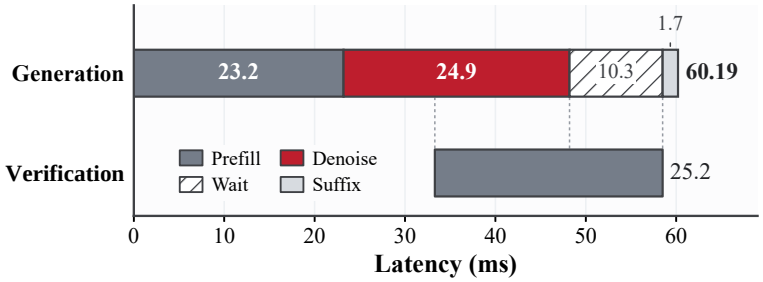

Figure 5: One decision cycle on an RTX 5090 with $\pi_{0.5}$ and N=4. Generation and verification share the same GPU. Encoding the pre-commit observation overlaps with candidate generation. Once the candidates are ready, scoring waits for this encoding to finish and then takes 1.7 ms. The full cycle takes 60.19 ms.

FlowRes configuration. Table 6 gives the values the reported runs use. All three share one noise sample across the candidates and all verification times, and all three score under o_{t+d-1} and commit at $t + d$.

Table 6: FlowRes settings for the simulation experiments. "Scored steps" is the range of j entering the sum, "weights" the w_j over that range, and "effective dims" the entries kept by $\mathbf{m}$.

Model	$\mathcal{T}$	Scored steps	w_j	Effective dims
Kinetix flow policy	0.2, 0.4, 0.6, 0.8	all 8 predicted	0.5^j	all
$\pi_{0.5}$ (LIBERO)	0.2, 0.4, 0.6, 0.8	first 5 (the executed ones)	uniform	7 of 32
GR00T N1.7	0.1, 0.3, 0.5, 0.7	all 16 predicted	0.5^j	7 of 132

Baseline implementation check. For the main Kinetix configuration in Table 1, setting N=1 uses RTC-guided generation without candidate selection. The resulting success rates differ from the RTC baseline by at most 0.7 percentage points across the reported delays.

Statistical reporting. For Table 1, each method is evaluated with 2,048 rollouts per Kinetix level and delay, giving 24,576 rollouts across the twelve levels. Table 2 uses the counts listed in Table 5. For Table 3, each method is evaluated with 500 episodes per LIBERO suite and delay. Benchmark averages are unweighted means over levels or suites. Full-rollout comparisons use separate runs for each method. The fixed-pool evaluation in Appendix D.2 instead compares selection rules at the same saved decision points. We report observed success rates and their differences without confidence intervals.

C Deployment Latency Breakdown

Figure 5 resolves the RTX 5090 entry of Table 4 into the stages of one decision cycle.

Generation begins at inference start with 23.2 ms of prefill over o_t, followed by 24.9 ms of flow integration. Generation and verification run concurrently on the same GPU. The pre-commit observation arrives one control step in, at 33.33 ms, and its prefill occupies the next 25.2 ms. Because that prefill depends only on the observation and not on the candidates, it overlaps the tail of generation instead of following it.

Candidate scoring starts only after both the candidates and the shared prefix KV cache are ready. The candidates become available first and wait about 10.3 ms for the cache before the 1.7 ms scoring pass. The full cycle ends at 60.19 ms. The time after candidate generation therefore includes both waiting and scoring. The segments are not independent: verification prefill shares the GPU with the tail of generation, so the generation time measured here already includes that contention and the figure does not separate the cost of producing four candidates from the cost of running verification alongside them. At 30 Hz the whole cycle still fits inside two control periods, which is the d=2 reported for both configurations on this GPU.

D Selector Ablations

Experimental controls. Tables 7 and 8 use the GR00T configuration of Table 3, including the same per-suite checkpoints, execution protocol, and episode count. The single-candidate baseline generates and executes one chunk. The three multi-candidate methods each generate N=8 candidates. Random selection chooses one uniformly at random. FlowRes on o_t scores candidates using the generation observation, while PACT-VLA uses the pre-commit observation o_{t+d-1}.

All methods use the same task set, initial-state set, inference delay, eight-action execution horizon, episode limit, and chunk-switching rule. The three multi-candidate methods also use the same generation procedure. Each method runs separately, and the candidate-sampling noise is not explicitly seeded. Candidates are generated from the observations encountered in each method's own rollout, which may differ after different actions are executed. These experiments therefore compare full-rollout success rather than selection from one shared candidate pool. The baseline column of Table 7 is the GR00T run reported in Table 3.

Selector comparison. At d=4, average success is 51.2% for single-candidate execution, 52.2% for random selection, 52.6% for FlowRes under the generation observation, and 56.4% for PACT-VLA. Scoring under the pre-commit observation yields higher observed success than same-observation scoring on all four suites.

Table 7: Selector comparison on GR00T N1.7 at d=4, with success rates reported in percent. All methods use the same evaluation protocol and initial-state set. The baseline generates one candidate, while the three multi-candidate methods each generate eight. Each method runs separately without sharing candidate pools.

Suite	Baseline	Random pick	FlowRes on o_t	PACT-VLA
Goal	52.2	55.8	54.2	58.2
Spatial	53.6	53.2	52.8	56.8
Object	62.6	64.8	64.6	67.8
LIBERO-10	36.4	35.0	38.6	42.6
Average	51.2	52.2	52.6	56.4

Effect of the verification observation across delays. Table 8 compares FlowRes under the generation and pre-commit observations. The observed average difference is larger at d=3 and d=4 than at d=2. At d=1, both variants use the same observation; the reported values come from independent runs.

Interpretation and scope. At d=1 the pre-commit observation coincides with the generation observation, and selection can help or hurt: per-suite differences in Table 3 span -1.8 to $+1.8$ on $\pi_{0.5}$ and -2.4 to $+0.2$ on GR00T N1.7. Under the five-step execution horizon of that table, the $\pi_{0.5}$ Spatial and Object suites came out negative at d=1 in all three evaluation seeds we ran, by -1.2 and -0.7 points on average.

Table 8: **PACT-VLA minus FlowRes on o_t for GR00T N1.7**, percentage points, by inference delay. At d=1 both arms score under the same observation.

Suite	d=1	d=2	d=3	d=4
Goal	−2.8	+1.2	+3.0	+4.0
Spatial	+1.0	+1.8	+5.0	+4.0
Object	+0.4	+0.4	+2.6	+3.2
LIBERO-10	−0.6	+0.8	+6.8	+4.0
Average	−0.5	+1.1	+4.3	+3.8

Table 9: Episode success (%) on Kinetix when changing only the observation used for FlowRes scoring. Results are averaged over 12 levels.

d	σ	Old (o_t)	PACT-VLA (o_{t+d-1})
2	0.1	85.44	89.40
3	0.1	75.04	85.56
4	0.1	62.02	77.16
4	0.0	64.69	79.64
4	0.2	52.07	64.35

D.1 Observation updates on Kinetix

Setting. We compare two FlowRes selectors on 12 Kinetix levels. Both use $N = 4$ candidates, the same checkpoint, candidate-generation procedure, scoring parameters, and execution schedule. They differ only in the observation used for verification: Old scores under the generation observation o_t, whereas PACT-VLA scores under the pre-commit observation o_{t+d-1}. We vary the inference delay d and execution-noise level σ. Table 9 reports episode success averaged over levels.

Results. At $\sigma = 0.1$, the difference grows with the inference delay, from 3.96 percentage points at $d = 2$ to 15.14 percentage points at $d = 4$. The gain remains positive without injected execution noise (14.95 points at $\sigma = 0$) and under stronger noise (12.28 points at $\sigma = 0.2$). These results support updating the scoring observation under inference delay. The benefit does not require injected execution noise.

D.2 Fixed-pool branch evaluation

Setting. At $d = 4$ and $\sigma = 0.1$, we evaluate 1,024 saved decision points per level and seed across 12 Kinetix levels and three seeds. Each point has a fixed pool of $N = 4$ candidates. Old and PACT-VLA select their candidates before any branch rollout. Each candidate is executed for four steps from the same saved state, after which all branches use the same continuation controller until termination. We perform eight independent continuations per candidate and evaluate uniform random selection, Old, and PACT-VLA on the same candidate pools. Results include all saved decision points.

Results. Average branch success is 61.18% for random selection, 61.07% for Old, and 61.62% for PACT-VLA. PACT-VLA improves over Old by 0.56 percentage points, with gains of 0.55, 0.49, and 0.63 points across the three seeds. Old remains close to random selection in observed success, while the pre-commit observation improves selection on unchanged candidate pools. This comparison isolates a single selection decision under a common continuation controller. Its gains are not directly comparable to episode-level gains from repeatedly applying the selector throughout a rollout.

E Real-Robot Data and Training

Demonstration data. We collect task-specific demonstrations through leader–follower teleoperation on the platform described in Section 4.2. Each demonstration records three camera streams at 480×640 resolution, together with the 14-dimensional robot state and action, at 30 Hz. Each task

uses only its own demonstrations. Table 10 summarizes the datasets, which contain 675 demonstrations totaling approximately 9.19 hours.

Table 10: Task-specific real-robot demonstration datasets.

Task	Demonstrations	Duration (h)	Mean length (s)
Toasting Bread	349	3.24	33.4
Loading Dishwasher	110	3.41	111.7
Pouring Coffee Beans	216	2.54	42.4
Total	675	9.19	

Base-policy training. We independently fine-tune a $\pi_{0.5}$ policy for each task using standard SFT for 40,000 gradient steps and evaluate the final checkpoint. Training uses AdamW with a batch size of 8, a peak learning rate of 10^{-5}, a 1,000-step linear warmup, and cosine decay to 1% of the peak rate. Only the action expert is updated; the vision-language backbone remains frozen. Naive Async, Old-FlowRes, and PACT-VLA use the same frozen task-specific SFT checkpoint. None of these three methods uses delay-aware or preference post-training. On the robot, Old-FlowRes and PACT-VLA each generate $N = 4$ candidates and use the verification flow times listed for $\pi_{0.5}$ in Table 6. Both methods score the first 25 actions with uniform weights, and the mask $\mathbf{m}$ retains all 14 bimanual action dimensions. This 25-action window determines which actions contribute to FlowRes, not when the controller switches chunks. Old-FlowRes uses the generation observation for scoring, while PACT-VLA uses the pre-commit observation. The policy predicts $H = 50$ actions, and the controller requests a new prediction when half of the current action queue remains, as described in Section 4.2.